Sensing and Bio-Sensing Research 38 (2022) 100535

Contents lists available at ScienceDirect

Sensing and Bio-Sensing Research

journal homepage: www.elsevier.com/locate/sbsr

Surface-enhanced Raman spectroscopy (SERS) for protein determination in human urine

Sultan Aitekenov [a], Alisher Sultangaziyev [a], Aisha Ilyas [a], Aigerim Dyussupova [a], Aigerim Boranova [a], Abduzhappar Gaipov [b], Rostislav Bukasov [a,*]

[a] Department of Chemistry, School of Sciences and Humanities (SSH) Nazarbayev University, Nur-Sultan, Kazakhstan
[b] Department of Medicine, School of Medicine, Nazarbayev University, Nur-Sultan, Kazakhstan

ARTICLE INFO

Keywords:
SERS
Raman spectroscopy
Commercial gold nanoparticles
Proteinuria
Chronic kidney disease CKD

ABSTRACT

Excessive protein excretion in human urine is an early and sensitive marker of diabetic nephropathy, primary and secondary renal disease. Kidney problems, particularly chronic kidney disease, remain among the few growing causes of mortality in the world. Therefore, it is important to develop efficient, expressive, and low-cost method for protein determination. Surface-enhanced Raman spectroscopy (SERS) methods are potential candidates to achieve those criteria. In this paper, the SERS method was developed to distinguish patients with proteinuria and the healthy group. Two types of commercial gold nanoparticles with a diameter of 60 nm and 100 nm were employed to prepare substrates for the analysis of 78 samples of unique patients. Data analysis by the PCA-LDA algorithm, and the ROC curves, gave results for diagnostic figures of merits. Sensitivity, specificity, accuracy, and AUC were 0.79, 0.89, 0.85, and 0.90 for the set with 60 nm Au NPs, respectively. Sensitivity, specificity, accuracy, and AUC were 0.79, 0.98, 0.90, and 0.91 for the set with 100 nm Au NPs, respectively. The results show the potential of SERS spectroscopy in differentiating between patients with proteinuria and healthy individuals for clinical diagnostics.

1. Introduction

Human urine is easily accessible while being non-invasive for patients, urine tests provide a plethora of information about patients' health. Health conditions detected by these tests range from cardiovascular and kidney diseases to various types of cancers [1–3]. Among many biomarkers in urine, excessive protein excretion is indicative of health conditions. Particularly, albumin (urinary protein) excretion of 30 to 300 mg a day, which is called microalbuminuria, is an early and sensitive marker of diabetic nephropathy [4], cardiovascular and renal disease [5]. One of the concerning public health problems worldwide is chronic kidney disease (CKD) because, and it remains among the few growing causes of mortality which made CKD the 13th leading cause of death in 2013 [6]. In 2017, CKD resulted in 1.2 million deaths worldwide, and together, deaths due to CKD or to CKD-attributable CVD (cardiovascular disease) accounted for 4.6% of all-cause mortality [7]. One of the other renal diseases that can be diagnosed by the protein in urine is - diabetic nephropathy, which is the most common cause of CKD that is responsible for >30% of the end-stage renal disease (ESRD) [8]. Raised albumin excretion of 30-300 mg/day along with the poor glycaemic control and the high arterial blood pressure are the symptoms of diabetic nephropathy [9]. Another important cause of ESRD is the glomerular disease, including nephrotic syndrome, that can be characterized by the high concentration of proteinuria (≥3.5 g/day) and hypoalbuminaemia (serum albumin ≤30 g/L) [10], and nephritic syndrome with the moderate concentration of proteinuria (<3.5 g/day) and hematuria (the presence of red blood cells in urine) [11]. Therefore, it is important to develop efficient, expressive, and low-cost method for protein content determination [12,13].

Surface-enhanced Raman spectroscopy is a technique that enhances Raman scattering [14]. The Raman spectrum arises from inelastic scattering of the laser light interactions with molecular vibrations, phonons, or other excitations in the system, resulting in the corresponding emission of photons. A simple flat metallic surface can already serve as an 'amplifier' of Raman signals for molecules deposited on it, albeit achieving a much lower level of amplification than that reached normally in metallic nanostructures [15]. The enhancement of Raman scattering is achieved by two mechanisms: typically the strongest one:

* Corresponding author.
E-mail address: rostislav.bukasov@nu.edu.kz (R. Bukasov).

https://doi.org/10.1016/j.sbsr.2022.100535
Received 9 June 2022; Received in revised form 6 October 2022; Accepted 13 October 2022
Available online 14 October 2022

electromagnetic enhancement (up to 10^{11}–10^{12}) [16], and the chemical enhancement by about factor 10–100. [17]. The total SERS enhancement can be as high as 10^{15} and it can allow the detection of a single analyte molecule [18]. [19,20]. In the last 40 years, AuNPs on gold, and AgNPs on silver have been the most widely employed SERS substrates due to providing broad and intense plasmon resonance in the wavelength range of interest for Raman [21]. Au nanoparticles are less susceptible to the oxidation than Ag [22], and more biocompatible [23], and demonstrates a strong plasmon excitation at higher wavelength closer to the 785 nm laser wavelength. Therefore, gold substrates have captured the most interest in its use in biotechnological systems [21].

Surface-enhanced Raman Spectroscopy-based methods are promising tools to be adopted in routine clinical tests in the future due to being fast, cheap, and label-free, as was stated in the comprehensive review about the quantification of proteins in human urine [3]. SERS methods were successful in the differentiation of urine of the control (healthy) group and the subject group with different types of cancers, such as breast, gastric, and ovarian [7,8]. Aitekenov et al. in the review about medical diagnostics and detection of biomarkers in biofluids by IR and Raman spectroscopy summarized the research literature on the topic in multiple tables [24]. One of those tables reported the calculated average diagnostic sensitivity, specificity, and accuracy (SSA) for SERS methods performed on human urine, which were calculated as 89%, 93% and 91% respectively, based on on a number of experimental papers, for example, by Hu et al. [25], Huttanus et al. [26], Ma et al. [27] and others. Please, see the full table S1 in the Supplementary Information. Those relatively good figures of merit were achieved by not only focusing on individual analytes and their corresponding peaks in the spectrum but rather on the spectrum as a whole. In other words, all features in the spectra of the healthy group and the subject group can be considered for their respective identification. Since biofluids contain hundreds of constituents and their quantity varies widely between individuals, even for healthy individuals, their spectra vary. Rather than focusing on individual peaks, they utilized multivariate analysis to take into consideration hundreds of variables (peaks), such as PCA-LDA (principal component analysis – linear discriminant analysis). In the current work, we used the same approach: the obtained SERS spectra from the control and the healthy group were analysed by PCA-LDA analysis to determine diagnostic sensitivity, specificity, accuracy, and other figures of merits. Commercial gold nanoparticles (AuNPs) drop casted on the commercially available gold-coated slides film make relatively inexpensive (at least in comparison to EBL (electron-beam lithography) based and some other nanofabricated substrates) and simple to prepare SERS substrate. Moreover, this kind of substrate, based on commercial AuNPs @ Au film, already demonstrated good effectiveness for the detection of various compounds including biomarkers [28–30]. Therefore, we decided to do urine screening for proteinuria on these substrates.

2. Materials and methods

2.1. Samples

Overall, 78 of 24-h urine tests of control (healthy) subjects and samples from patients with proteinuria were collected by hospital. The protein concentrations varied greatly between individuals: 42 individuals had protein concentration below 0.15 g/L, 36 patients had protein concentration above 0.15 g/L. Written consent from all patients were received. The hospital performed routine urinary tests to determine protein concentrations, volume of urine, and concentrations of other substances. The samples were stored at −20 °C.

2.2. Chemicals and equipment

Commercial 60 nm gold nanoparticles in PBS and 100 nm gold nanoparticles in PBS were purchased from Sigma-Aldrich (USA) with reported ranges 61–73 nm and 100–125 nm, respectively. Gold coated test slides (gold substrates) were purchased from EMF Dynasil (USA). Raman spectra were obtained with the confocal Raman microspectrometer The Horiba LabRam Evolution. Pictures from a scanning electron microscope were obtained from Zeuss Crossbeam 540.

2.3. SEM characterisation

SEM acquisition parameters: accelerating voltage EHT = 5.00 k*V*, working distance WD = 5.1 mm, I probe = 139 pA, ESB grid = 833 V.

2.4. Substrate preparation

The composite AuNP@gold film substrate was prepared in a similar way as it was described previously [28,30]. About of 1 mL of suspension of commercial gold nanoparticles of 60 or 100 nm diameter (OD =1.0) were centrifuged for 5 min at 3500*g* and 1500 g respectively, and the supernatant was removed and displaced with the similar amount of ultra-pure water. This cycle was repeated 3 times. 15 μL (microliters) of solution of gold nanoparticles were drop casted on the gold coated test slides at the room temperature and let dry. Urine samples were thawed after storage in the freezer. Then 15 μL of urine samples were drop casted on the obtained solid spots from nanoparticles. Each sample was prepared in triplicates to maximize reproducibility of the measurements.

2.5. Spectra acquisition

Raman spectra acquisition was performed with the following parameters: laser excitation wavelength 785 nm, range 400 to 1800 cm^{-1}, grating 600 g/mm, magnification x10, ND filter 100%, acquisition time 16 s. We did systematic, ensemble SERS measurements, when spectra from 3 different spots were taken. The first spot was taken near the middle of a try droplet, and the second and the third spots were (0,200) and (200,0) away from the first in the (x, y) axis respectively measured in micrometers. For each spot 12 spectra were averaged, therefore 36 spectra were averaged for each urine sample.

2.6. Spectra processing and data analysis

All spectra processing and data analysis were performed on MATLAB. The obtained spectra were processed in the order:

1. ALS (asymmetric least squares algorithm) – removes fluorescence background.
2. Median filter – removes outliers.
3. Savitsky-Golay smoothing algorithm – preserves intensities, removes unwanted features [31].

The processed spectra were analysed by PCA - DA (principal component analysis –discriminant analysis) method and ROC (receiver operating characteristic) curves to construct a statistical model. The statistical model was used for calculations of diagnostic sensitivity, specificity, accuracy, and other figures of merits. Diagnostic sensitivity, specificity and accuracy are commonly reported in biomedical papers. Sensitivity is a measure of how well a test can identify true positives and specificity is a measure of how well a test can identify true negatives while accuracy is how close or far off a given set of measurements are to their true value. The exact formulas are as follows:

$$sensitivity = \frac{true\ positive}{positive}$$

$$specificity = \frac{true\ negative}{negative}$$

$$accuracy = \frac{true\ positive + true\ negative}{positive + negative}$$

3. Results and discussions

After Raman measurements were performed, some substrates were imaged by a scanning electron microscope (SEM), see Fig. 1. Fig. 1 (A) and (B) show typical SEM images of the same kind of substrate surface but with 60 nm and 100 nm Au NPs respectively, magnification x50000. SEM images demonstrate the availability of Au NPs on the sample and those nanoparticles are relatively uniform in their size. Statistical analysis performed on SEM images gives mean and standard deviation for 60 nm nanoparticles as 62 and 3 nm, respectively, and for 100 nm nanoparticles as 103 and 11 nm, respectively, more in the Supplementary Information. Other objects in SEM images such as crystals are not uniform in size and their mean and standard deviation are 980 and 460 nm, respectively.

Also, those SEM images of the substrate demonstrated that gold nanoparticles have a bit non-ideal spherical shape, and most nanoparticles are associated into dimers, trimers, and larger oligomers. This association must increase the total number of active SERS hot spots in the substrate and boost its enhancement factor, as it was reported for the study of SERS signal on nanoparticle dimers and trimers vs SERS signal on single nanoparticles [32,33].

There are a number of works showing higher enhancement factor for nanoparticles with bigger size [34,35]. We would expect that increasing gold nanoparticles particle size from 40 to 100 nm produces stronger LSPR for an excitation of 785 nm and produces larger SERS signals due to optical absorption and scattering of the substrates, while the same trend was experimentally observed for 35 to 65 nm silver nanoparticles with 633 nm laser excitation, as reported by He et al. [34], the same trend for Au(core)-Ag(shell) nanoparticles within 38, 53, and 90 nm was observed by Sugawa et al. [35]. We chose 60 nm and 100 nm Au NPs also because our preliminary measurements of 10 patient samples, demonstrated lower performance with smaller particle size (40 nm), please see the Supplementary Information.

The typical collected spectra for samples with high and low protein concentration before and after background subtraction are shown on Fig. 1 in the Supplementary Information. Fig. 2 shows three averaged SERS spectra: one of urine samples with low protein concentration, another one of samples with high protein concentration and the spectrum of their difference. The initial threshold to distinguish between high and low protein concentration in urine is 150 mg/L of protein, making 36 patient samples in “low” and 42 patient samples in “high” protein concentration category. The wavelength range is 960–1700 cm^{-1}. The figures look similar for both substrates made of 60 and 100 nm diameter gold nanoparticles, demonstrating strong band in the region 1310–1400 cm^{-1}. We have noticed in our Raman spectra an artifact: a periodic interference that mostly affected spectra in the range 400–900 cm^{-1}. The signal artifact in this range, likely from reflected light reaching the CCD is present even in the spectra of bare gold film, which should be flat, but nevertheless creates an oscillating signal as demonstrated on Fig. 2 in the Supplementary Information· Partially because of the mentioned problem we have analysed Raman intensities in the range higher than 900 cm^{-1} for statistical discrimination. Also, statistical models processing our data, showed better performance in terms of AUC (area under the curve in the ROC curve) values when the range 960–1700 cm^{-1} was selected in comparison to ranges starting from lower wavenumbers. Moreover, we believe that this range contains the most important vibrational frequencies for protein determination as explained further in the text, particularly in Table 1.

Comprehensive band assignment in the human urine matrix was performed by Moreira et al. [36], see Table 1. Dingari et al. experimentally showed strong peaks for drop coated albumin for the following wavenumbers: 1655 cm^{-1} amide-I band, 1447 cm^{-1} CH2 deformation band, 1002 cm^{-1} phenylalanine band [37]. Though specific correlations with substances were not provided, Zong et al. suggest that peaks at 1079, 1185, 1287, and 1383 cm^{-1} are specific to the population with CKD since these peaks were not reported in some other research groups that studied human urine with individuals with other health conditions [38]. In another similar research dedicated to proteinuria by Chen et al., the peaks at ~1150 and 1585 cm^{-1} are the most intense peaks [39]. While authors did not assign the peak at 1150 cm^{-1} to protein substances, they assigned peaks at 1230–1282 to amide III, 1447 cm^{-1} to phospholipids, and the peaks at 1585, 1615, 1654 cm^{-1} for tyrosine and tryptophan. Saatkamp et al. experimentally showed that the peaks at 527, 1006, and 1160 cm^{-1} indicate the presence of urea, with attribution assigned to the symmetric stretching peak C—N for the peak at 1006 cm^{-1} and C—NH_2 and C═O stretching and confirmed by their literate study [40]. Mukanova et al. reported the similar strong peak at

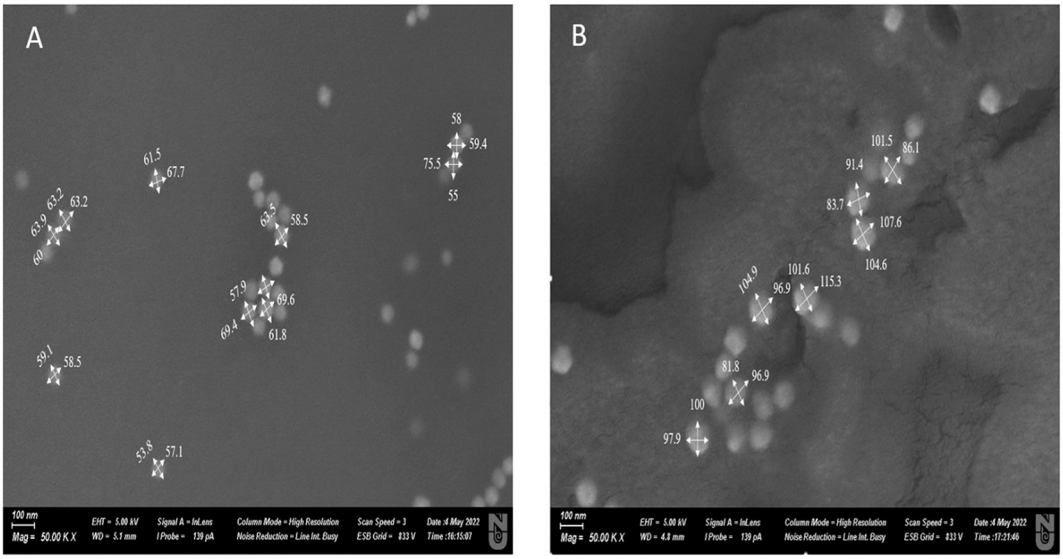

Fig. 1. SEM pictures of urine solids on 60 nm and 100 nm Au NPs on the gold substrate. (A) The SEM image of a sample with 60 nm Au NPs with magnification of 50.000. (B) The SEM image of a sample with 100 nm Au NPs with magnification of 50.000. Statistical analysis performed on SEM images gives mean and standard deviation for 60 nm nanoparticles as 62 and 3 nm, respectively, and for 100 nm nanoparticles as 103 and 11 nm, respectively. (For interpretation of the references to colour in this figure legend, the reader is referred to the web version of this article.)

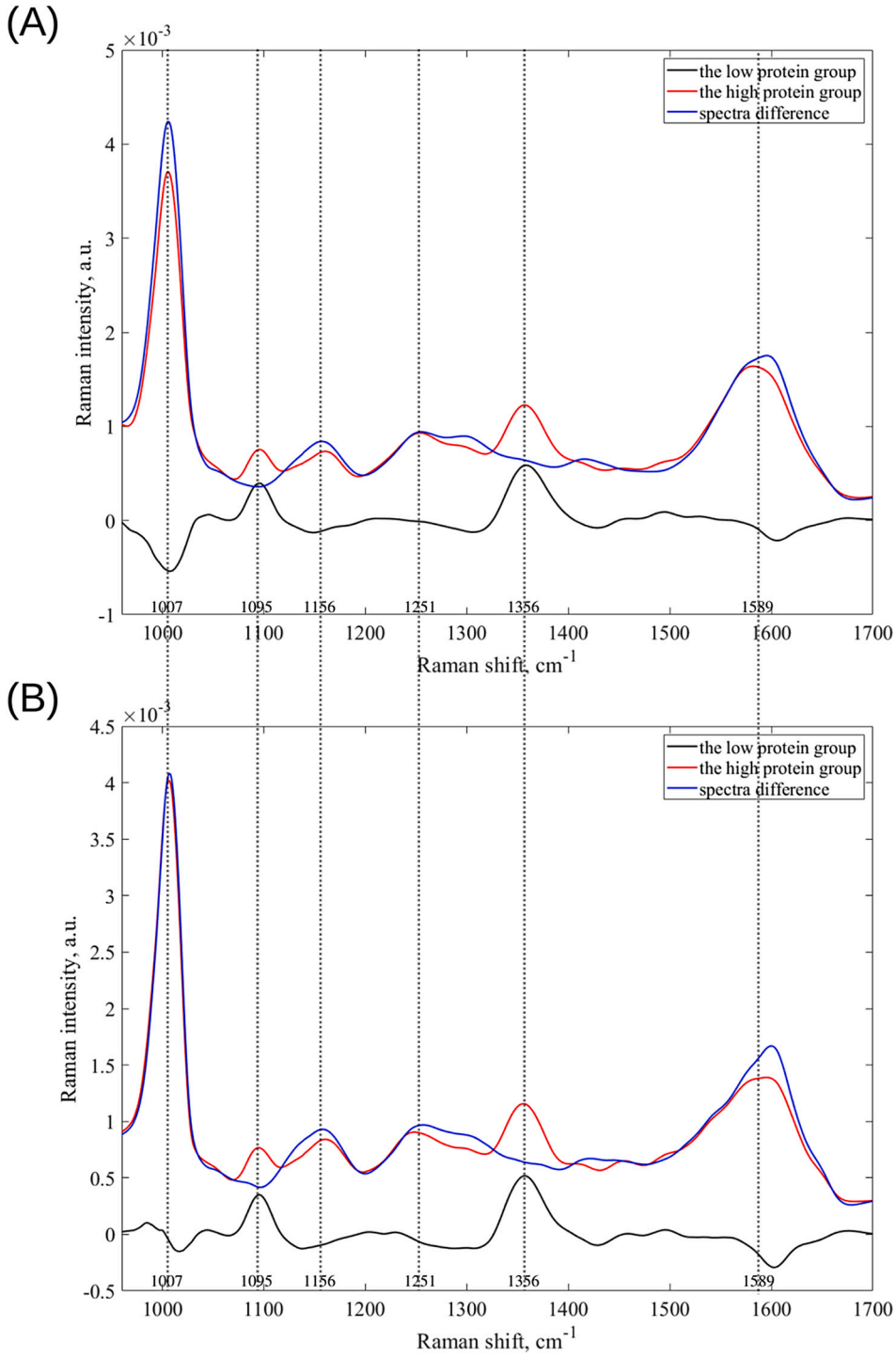

Fig. 2. Mean SERS spectra of urine samples with the low and the high protein groups with the spectrum of their difference. The protein threshold is 150 mg/L. (A) Urine samples with the gold substrate with 60 nm Au NPs. (B) Urine samples with the gold substrate with 100 nm Au NPs. (For interpretation of the references to colour in this figure legend, the reader is referred to the web version of this article.)

1007 cm^{-1} for urea [30]. In the Supplementary Info, we attached some figures with SERS/Raman spectra of albumin and urea. Overall, the most intense peak in urine samples is located at ~1003 cm^{-1} which corresponds to C—N symmetric stretching, that primarily comes from urea, other peaks in urine are much weaker and located at 1178, 1466, 1540, 1576, and 1630 cm^{-1} [41].

Our experimental results show two strong peaks at 1094 and 1355 cm^{-1}, a medium intensive peak at 1044 cm^{-1}, and weak peaks at 1167, 1454 and 1493 cm^{-1}, see in Fig. 2. Our peaks at 1094 and 1355 cm^{-1} are relatively close to that of reported by Zong et al. at 1079 and 1383 cm^{-1}, respectively. Those peaks might be specific to the group with proteinuria. Close to our weak peaks at 1167, 1454 and 1493 cm^{-1} are reported for healthy subjects as well, for example [41].

Discrimination between the low protein group and the high protein group was further conducted by PCA-LDA and ROC curves [57,58]. Fig. 3 shows PC related graphs for the set with 60 nm Au NPs. Graphs of the first 9 PC coefficients versus Raman shift are presented in Fig. 3 (A) since they account for the most amount of the explained variability.

Table 1
Spectra interpretation of the human urine by Moreira et al. [36].

Peak position, cm^{-1}	Component, attribution, and literature found
983	Phosphate (P—H bending and P—O stretching) [42]
1006	Urea (N-C-N stretching) [43–46]
1050	Creatine (1054); hydroxybutyrate (1060) from ketone bodies [47–50]
1079	Nitrogenous compounds (CN stretching from primary amines) [51,52]
1159	Urea (NH_2 rocking) [43–45,53]
1344	Hydroxybutyrate from ketone bodies [47,51,54]
1420	Creatinine (1420); creatine (1424); acetoacetate (1422) from ketone bodies [48,49,53,55]
1456	Hydroxybutyrate (1443 and 1456) and acetoacetate (1444) from ketone bodies [49,50,56]
1608	Urea [44,45]
1650	Water (H-O-H bending mode) [54]

Together first 9 coefficients account for 97.0% of the explained variability. Some high protein samples in Fig. 3 (B,C) are located away from the rest, while most samples are clustered around the line. The area under the ROC curve (AUC) was taken as the main measure of test performance. In our analysis, the protein threshold was set to 150 mg/L and 300 mg/L for three reasons. The first reason is that, historically, protein excretion of >150 mg/day was regarded as abnormal [59]. Though a man excretes about 1.5 L of urine a day, the threshold of 150 mg/L divides samples into roughly equal groups – 42 for the high protein group, and 36 for the low protein group making 78 samples in total, while the threshold of 300 mg/L divides samples into 44 for the high protein group, and 34 for the low protein group. Lastly, urine reagent strip devices that are commonly used in medical diagnostics have a higher threshold of about 300 mg/L [60], and we chose to pick threshold values lower and equal to 300 mg/L.

Firstly, we used ROC (receiver operating characteristic) curves to decide on number of PC components. Particularly, AUC values greatly depend on multiple factors, and one of them is PC components. As an example, Fig. 4 shows ROC curves of urine samples on the gold substrate with 60 nm and 100 nm Au NPs at the protein threshold of 150 mg/L. Table 2 below shows how sensitivity, specificity, accuracy, AUC, and other variables varies with number of PC components for experimental sets with the protein threshold of 150 mg/L. Similar information for the threshold of 300 mg/L is given in Supplementary information. Those are with 60 nm Au NPs and 100 nm Au NPs on the gold substrate with two protein threshold numbers 150 mg/L and 300 mg/L. Also, those tables contain information on a confusion matrix. A confusion matrix is a summary of prediction results on a classification problem that are divided into True Positives (TP), True Negatives (TN), False Positives (FP) and False Negatives (FN). Sensitivity, specificity, accuracy, and confusion matrices were calculated from respective ROC curves by maximizing sum of sensitivity and specificity. For example, Fig. 4 represents a ROC curve that shows relationship between sensitivity and 1-specificity. By taking the sum of sensitivity and specificity from that curve, the maximum sensitivity and specificity could be found, along with values for accuracy and values for a confusion matrix.

If we look solely on AUC vs PC for an individual experimental set, AUC values are rising, but that results in overfitting data because AUC one-leave-out starts to decrease from certain PC values. One-leave-out algorithm was used for avoidance of over-optimization the model with excessive numbers of PC components. For 150 mg/L, AUC values are better for 60 nm Au NPs, than for 100 nm Au NPs, at least for up to 13 PC components. As a result, sensitivity, specificity, and accuracy tend to be better for 60 Au NPs in this case. However, for 300 mg/L, AUC values are better for 100 nm Au NPs than for 60 nm Au NPs. In general, though, results for both nanoparticles are similar.

The best results were picked by the reference to the sum of AUC and AUC leave-out-values along with the total variance explained. For 60 nm Au NPs, the best results were picked for 15 PC components for both thresholds. As for 100 nm Au NPs, 13 PC components were picked. For 150 mg/L and 60 nm Au NPs sensitivity, specificity, accuracy, and AUC are 0.976, 0.667, 0.833, 0.905, respectively. For 150 mg/L and 100 nm Au NPs sensitivity, specificity, accuracy, and AUC are 0.762, 0.972, 0.859, 0.890, respectively. For 300 mg/L and 60 nm Au NPs sensitivity, specificity, accuracy, and AUC are 0.794, 0.886, 0.846, 0.899, respectively. For 300 mg/L and 100 nm Au NPs sensitivity, specificity, accuracy, and AUC are 0.794, 0.977, 0.897, 0.913, respectively. Among those four sets of diagnostic figures, some contain high sensitivity and some high specificity. Moreover, we performed three additional statistical tests. For the first test, the data for sets with 60 nm and 100 nm were combined. The results were largely the same. Sensitivity, specificity, accuracy, and AUC were 0.857, 0.778, 0.821, 0.884, respectively. The second test consists of omitting samples within 130 and 170 mg/L because there might be problems of how accurate the protein concentration in urine can be measured. Only 3 samples were between that range and omitting them did not change diagnostic figures meaningfully. In this case, for 150 mg/L and 60 nm Au NPs sensitivity, specificity, accuracy, and AUC are 0.968, 0.69, 0.838, 0.909, respectively. Lastly, we applied the same calculation principles to analyze whether the peak of 1355 cm^{-1} is predictive by itself. SERS intensities between the Raman shift range of 1355 ± 10 cm^{-1} with 15 PC components yielded AUC values of 0.66 and 0.58 for the data sets obtained with 60 and 100 nm Au NPs respectively. Therefore, the Raman spectrum, which we used (960 to 1800 cm^{-1}), has much better predictive power.

To understand the competitiveness of our results we performed a literature search among studies containing SERS/Raman analysis of urine or detection of proteinuria. Table 3 is a summary of experimental papers on protein detection in human urine and Raman analysis of human urine. Firstly, we compared our results for the detection of proteinuria with other techniques like the dipstick test, spot urine protein-creatinine ratio, and ^{1}H NMR. Comparison with commonly used urine dipstick test showed that our method outperforms it both in terms of sensitivity and specificity with the higher area under the ROC curve [61]. The alternative method for detection of proteinuria with protein to creatinine ratio by Beckman Synchron also showed lower figures of merit than our method [62]. And more novel method of proteinuria detection with ^{1}H NMR yielded slightly lower accuracy than our method and significantly lower AUC [63]. In addition, we were able to get a lower threshold value of 150 mg/L compared to these methods, which reported protein concentration thresholds of 300 mg/L [61,62], and 3000 mg/day [63]. Thus, the use of SERS for the detection of proteinuria is not only more sensitive and accurate but also can distinguish lower protein concentrations.

Finally, we compared the performance of our method with studies analyzing urine by Raman spectroscopy, like ours. The figures of merit of these studies used for comparison can be seen in Table 3. For example, a study by Zong et al. about the diagnosis of chronic kidney disease by SERS analysis of urine showed a bit lower level of accuracy than accuracy calculated in our research (82% vs 86% average for the current paper) [38]. Moreover, our results were at least on par or a bit better in comparison with results for the detection of chronic renal failure (accuracy 85%) [64], coronary heart disease, where reported accuracy was 83% [65], and bladder cancer where accuracy was 80% [66]. This suggests that the use of Raman spectroscopy for urine analysis has similar performance in detection across different diseases/conditions and thus there is a potential for simultaneous screening for different pathologies. Also, since apparently, we have obtained comparatively high AUC, accuracy and other FOMs, the Table 3 demonstrates a relative efficiency of our SERS method for the screening of proteinuria.

4. Conclusion

The results show the potential of SERS spectroscopy in

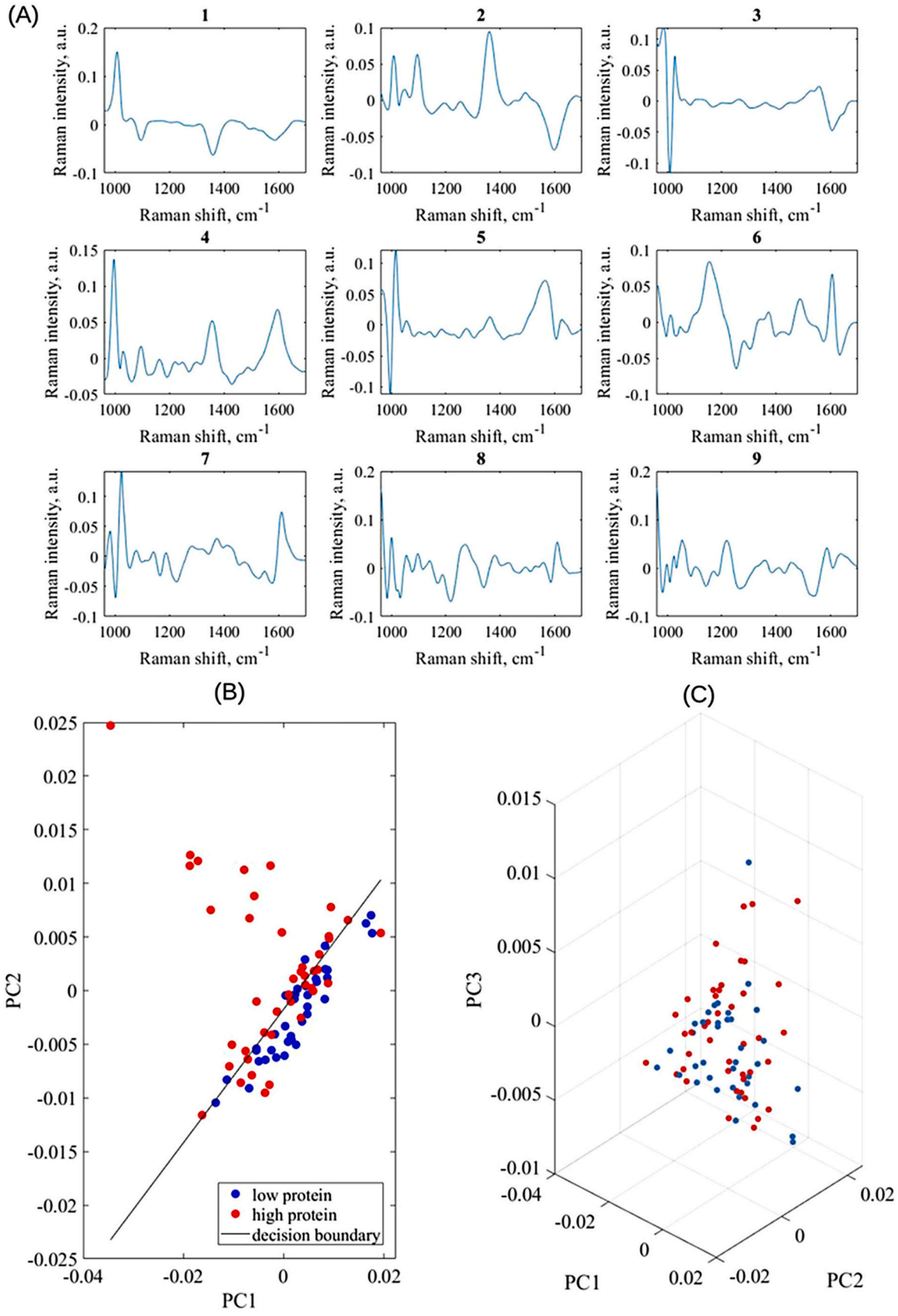

Fig. 3. PC related graphs for the set with 60 nm Au NPs. Protein threshold is 150 mg/L. Low protein samples are colored in blue. High protein samples are colored in red. (A) Graphs of the first 9 PC coefficients versus Raman shift. The corresponding PC component is written above each graph. (B) PC1 vs PC2 graph with a line separating low protein (blue) and high protein (red) samples. (C) PC1 vs PC2 vs PC3 graph. (For interpretation of the references to colour in this figure legend, the reader is referred to the web version of this article.)

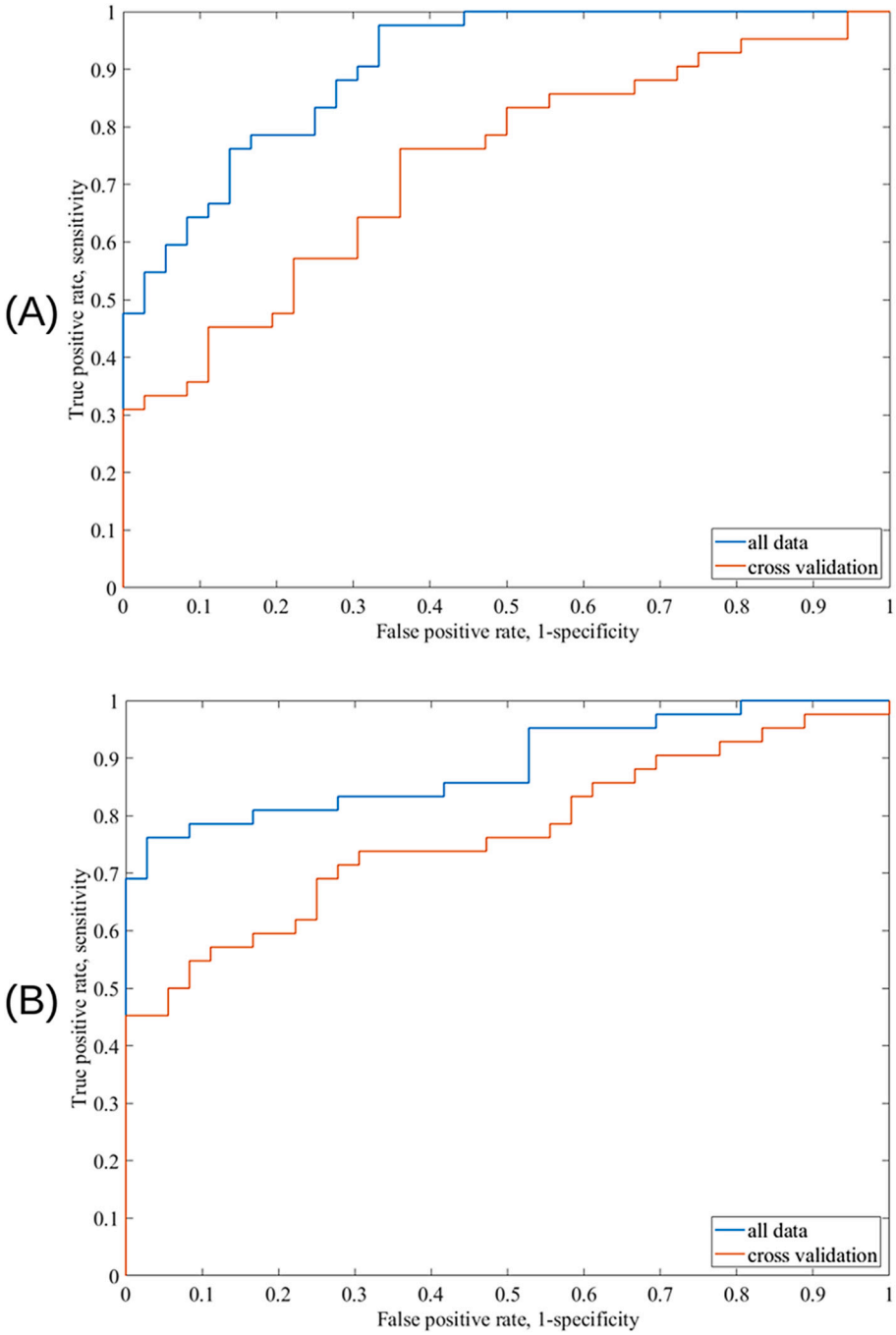

Fig. 4. ROC curves of urine samples on the gold substrate with 60 nm (A) and 100 nm (B) Au NPs. The protein threshold equals 150 mg/L. The orange line shows ROC curve with one-leave-out algorithm. The blue line treated all data as a training set. The ROC curve for 60 nm Au NPs is based on logistic regression with 15 PC components. AUC equals to 0.905, AUC with the cross validation is 0.733. The ROC curve for 100 nm Au NPs is based on logistic regression with 13 PC components. AUC equals to 0.890, AUC with the cross validation is 0.767. (For interpretation of the references to colour in this figure legend, the reader is referred to the web version of this article.)

differentiating between patients with proteinuria and the healthy group for clinical diagnostics. The employed approach with 60 nm and 100 nm Au NPs achieved good discrimination values as measured with AUC in the ROC curves. Data analysis by PCA-DA algorithm, and the ROC curves, gave results for diagnostic figures of merits. Using diagnostic threshold protein concentration 300 mg/L we obtained sensitivity, specificity, accuracy, and AUC: 0.79, 0.98, 0.90 and 0.91, respectively, for the measurements on 100 nm Au NPs@gold film substrate. The same FOMs are a bit lower for the measurement on 60 nm Au NPs: 0.79, 0.89, 0.85 and 0.90, respectively. Decreasing diagnostic protein threshold to 150 mg/L for measurements on 60 nm Au NPs can bring some improvement in sensitivity (to 0.976) at the expense of decreasing specificity (to 0.67), while accuracy and AUC do not show significant change (0.83 and 0.905 respectively). Overall, 300 mg/L protein diagnostic threshold and 100 nm diameter gold nanoparticles on gold film measured with 785 nm laser excitation appears as an optimal combination providing the best balance between sensitivity and specificity in this SERS based method of proteinuria diagnostics.

Finally, the described SERS method of protein content analysis in human urine is relatively inexpensive and fast. However, as an alternative to gold film in Au NPs@gold film substrate, we are planning to test less expensive and more available substrates with this method of protein urea detection, such as silicon or/and aluminum foil.

Author contributions

Bukasov Rostilsav is responsible for general idea and management/directing/correcting of research and manuscript writing. Aitekenov

Table 2
Data analysis output by PCA, LDA, ROC, obtained with SERS on 60 nm and 100 nm diameter Au NPs for the protein threshold concentration of 150 mg/L. Samples total - 78, above the threshold - 42, below - 36. Best values highlighted in grey.

Au NPs diameter	PC components	Total variance explained, %	Sensitivity	Specificity	Accuracy	AUC	AUC one-leave-out	TP	TN	FP	FN
	1	51.9	0.476	0.806	0.628	0.628	0.585	20	29	7	22
	3	85.3	0.690	0.889	0.782	0.791	0.732	29	32	4	13
	5	92.2	0.714	0.806	0.756	0.804	0.722	30	29	7	12
	7	95.2	0.762	0.806	0.782	0.810	0.678	32	29	7	10
	9	97.0	0.810	0.778	0.795	0.866	0.766	34	28	8	8
60 nm	11	97.8	0.857	0.778	0.821	0.870	0.749	36	28	8	6
	13	98.4	0.857	0.778	0.821	0.873	0.716	36	28	8	6
	15	98.8	0.976	0.667	0.833	0.905	0.733	41	24	12	1
	17	99.1	0.857	0.861	0.859	0.913	0.706	36	31	5	6
	19	99.3	0.833	0.861	0.846	0.912	0.690	35	31	5	7
	21	99.5	0.857	0.833	0.846	0.909	0.662	36	30	6	6
	1	46.5	0.667	0.528	0.603	0.551	0.443	28	19	17	14
	3	83.2	0.548	0.833	0.679	0.745	0.667	23	30	6	19
	5	90.6	0.762	0.722	0.744	0.773	0.661	32	26	10	10
	7	94.2	0.667	0.861	0.756	0.791	0.650	28	31	5	14
	9	96.0	0.548	1.000	0.756	0.835	0.708	23	36	0	19
100 nm	11	97.1	0.667	0.944	0.795	0.872	0.735	28	34	2	14
	13	97.9	0.762	0.972	0.859	0.890	0.767	32	35	1	10
	15	98.4	0.786	0.917	0.846	0.889	0.737	33	33	3	9
	17	98.8	0.762	0.972	0.859	0.904	0.717	32	35	1	10
	19	99.1	0.786	1.000	0.885	0.947	0.771	33	36	0	9
	21	99.3	0.905	0.944	0.923	0.958	0.769	38	34	2	4

Note: Accuracy = (TP + TN)/(TP + TN + FP + FN); Sensitivity = (TP)/(TP + FN); Specificity = (TN)/(TN + FP). TP – true positive, TN – true negative, FP – false, FN – false negative.

Table 3
Summary table of experimental papers on protein detection in human urine.

Paper	Method	Condition (threshold)	Sensitivity	Specificity	Accuracy	AUC
current paper	SERS, 60 nm Au NPs	Proteinuria	0.976	0.667	0.833	0.905
	SERS, 100 nm Au NPs	150 mg/L	0.762	0.972	0.859	0.890
current paper	SERS, 60 nm Au NPs	Proteinuria	0.794	0.886	0.846	0.899
	SERS, 100 nm Au NPs	300 mg/L	0.794	0.977	0.897	0.913
Nielsen et al. [61]	Urinary dipstick test	Proteinuria	0.727	0.557	NA	0.762
Rizk et al. [62]	Spot urine protein-creatinine ratio	Proteinuria	0.804	0.688	NA	0.82
Kalantari et al. [63]	^{1}H NMR	Proteinuria	0.8	0.8	0.8	0.714
Zong et al. [38]	SERS	Chronic kidney disease	0.78	0.86	0.818	0.886
Chen et al. [64]	Raman spectroscopy	Chronic renal failure	0.833	0.857	0.846	NA
Yang et al. [65]	SERS	Coronary heart disease	0.9	0.789	0.828	NA
Huttanus et al. [66]	Raman spectroscopy	Bladder cancer	0.824	0.795	0.804	NA

Sultan responsible for writing the bulk of the research paper, development of data analysis procedure and training /supervising of some other participants in sample preparation and measurements. Alisher Sultangaziev is responsible for writing some part of introduction as well as part of discussion and doing some sample preparation, measurement and data analysis. Aisha Ilyas, Aigerim Dyussupova, Aigerim Boranova participated in sample preparation, Raman and SEM measurements as well as some basic data analysis. Dr. Abduzhappar Gaipov provided funding of the experimental work and gave a few valuable suggestions about the paper.

Funding statement

The authors of this paper acknowledge funding from the Nazarbayev University Collaborative Research Program (CRP) for 2020–2022 (Funder Project Reference: 091019CRP2105).

Declaration of Competing Interest

The authors declare that they have no known competing financial interests or personal relationships that could have appeared to influence the work reported in this paper.

Data availability

Data will be made available on request.

Acknowledgements

The trial has been approved by http://ClinicalTrials.gov (Trial registration ID NCT04311684). The date of registration was March 17, 2020.

Appendix A. Supplementary data

Supplementary data to this article can be found online at https://doi.org/10.1016/j.sbsr.2022.100535.

References

[1] K.V. Hackshaw, J.S. Miller, D.P. Aykas, L. Rodriguez-Saona, Vibrational spectroscopy for identification of metabolites in biologic samples, Molecules 25 (Jan. 2020), https://doi.org/10.3390/molecules25204725 no. 20, Art. no. 20.
[2] M.J. Baker, et al., Developing and understanding biofluid vibrational spectroscopy: a critical review, Chem. Soc. Rev. 45 (7) (Mar. 2016) 1803–1818, https://doi.org/10.1039/C5CS00585J.
[3] S. Aitekenov, A. Gaipov, R. Bukasov, Review: detection and quantification of proteins in human urine, Talanta 223 (Feb. 2021), 121718, https://doi.org/10.1016/j.talanta.2020.121718.

[4] G.C. Viberti, R.J. Jarrett, U. Mahmud, R.D. Hill, A. Argyropoulos, H. Keen, Microalbuminuria as a predictor of clinical nephropathy in insulin-dependent diabetes mellitus, Lancet 319 (8287) (Jun. 1982) 1430–1432, https://doi.org/10.1016/S0140-6736(82)92450-3.

[5] H.J. Lambers Heerspink, J.W. Brinkman, S.J. Bakker, R.T. Gansevoort, D. de Zeeuw, Update on microalbuminuria as a biomarker in renal and cardiovascular disease, Curr. Opin. Nephrol. Hypertens. 15 (6) (Nov. 2006) 631–636, https://doi.org/10.1097/01.mnh.0000247496.54882.3f.

[6] C. Murray, Global, regional, and national age–sex specific all-cause and cause-specific mortality for 240 causes of death, 1990–2013: a systematic analysis for the Global Burden of Disease Study 2013, Lancet 385 (9963) (Jan. 2015) 117–171, https://doi.org/10.1016/S0140-6736(14)61682-2.

[7] E.F. Carney, The impact of chronic kidney disease on global health, Nat. Rev. Nephrol. 16 (5) (May 2020) 251, https://doi.org/10.1038/s41581-020-0268-7.

[8] C.O. Alebiosu, O.E. Ayodele, The global burden of chronic kidney disease and the way forward, Ethn. Dis. 15 (3) (Aug. 2005) 418–423.

[9] B.A. Perkins, L.H. Ficociello, K.H. Silva, D.M. Finkelstein, J.H. Warram, A. S. Krolewski, Regression of microalbuminuria in type 1 diabetes, N. Engl. J. Med. 348 (23) (Jun. 2003) 2285–2293, https://doi.org/10.1056/NEJMoa021835.

[10] S.A. Politano, G.B. Colbert, N. Hamiduzzaman, Nephrotic syndrome, Prim. Care 47 (4) (Dec. 2020) 597–613, https://doi.org/10.1016/j.pop.2020.08.002.

[11] M.S. Hashmi, J. Pandey, Nephritic Syndrome, StatPearls Publishing, Treasure Island (FL), 2021 [Online]. Available: http://europepmc.org/abstract/MED/32965911.

[12] A. Gaipov, et al., Development and validation of hybrid Brillouin-Raman spectroscopy for non-contact assessment of mechano-chemical properties of urine proteins as biomarkers of kidney diseases, BMC Nephrol. 21 (1) (Dec. 2020) 229, https://doi.org/10.1186/s12882-020-01890-x.

[13] A. Gaipov, et al., P0666 Brillouin AND raman spectroscopies for non-contact assessment of mechano-chemical properties of urinary proteins: a proof of concept study, in: *Proceedings of the European Dialysis and Transplant Association - European Renal Association. European Dialysis and Transplant Association - European Renal Association. Congress*, vol. 35, no. Supplement_3, Jun. 2020, https://doi.org/10.1093/ndt/gfaa142.P0666.

[14] A. Bonifacio, S. Cervo, V. Sergo, Label-free surface-enhanced Raman spectroscopy of biofluids: fundamental aspects and diagnostic applications, Anal. Bioanal. Chem. 407 (27) (Nov. 2015) 8265–8277, https://doi.org/10.1007/s00216-015-8697-z.

[15] E.C. Le Ru, P.G. Etchegoin, Chapter 1 - A quick overview of surface-enhanced Raman spectroscopy, in: E.C. Le Ru, P.G. Etchegoin (Eds.), Principles of Surface-Enhanced Raman Spectroscopy, Elsevier, Amsterdam, 2009, pp. 1–27, https://doi.org/10.1016/B978-0-444-52779-0.00007-6.

[16] E.C. Le Ru, E. Blackie, M. Meyer, P.G. Etchegoin, Surface enhanced Raman scattering enhancement factors: a comprehensive study, J. Phys. Chem. C 111 (37) (Sep. 2007) 13794–13803, https://doi.org/10.1021/jp0687908.

[17] L. Guerrini, D. Graham, Molecularly-mediated assemblies of plasmonic nanoparticles for surface-enhanced Raman spectroscopy applications, Chem. Soc. Rev. 41 (21) (2012) 7085–7107, https://doi.org/10.1039/C2CS35118H.

[18] A. Fahes, A. En Naciri, M. Navvabpour, S. Jradi, S. Akil, Self-assembled ag nanocomposites into ultra-sensitive and reproducible large-area SERS-active opaque substrates, Nanomaterials 11 (8) (2021), https://doi.org/10.3390/nano11082055.

[19] K. Kneipp, et al., Single molecule detection using surface-enhanced Raman scattering (SERS), Phys. Rev. Lett. 78 (9) (Mar. 1997) 1667–1670, https://doi.org/10.1103/PhysRevLett.78.1667.

[20] S. Nie, S.R. Emory, Probing single molecules and single nanoparticles by surface-enhanced Raman scattering, Science 275 (5303) (Feb. 1997) 1102–1106, https://doi.org/10.1126/science.275.5303.1102.

[21] S. Hong, X. Li, Optimal size of gold nanoparticles for surface-enhanced Raman spectroscopy under different conditions, J. Nanomater. May 2013 (2013), 790323, https://doi.org/10.1155/2013/790323.

[22] C.J. Murphy, et al., Gold nanoparticles in biology: beyond toxicity to cellular imaging, Acc. Chem. Res. 41 (12) (Dec. 2008) 1721–1730, https://doi.org/10.1021/ar800035u.

[23] J. Kneipp, H. Kneipp, B. Wittig, K. Kneipp, 'Novel optical nanosensors for probing and imaging live cells', *nanomedicine: nanotechnology*, Biol. Med. 6 (2) (Apr. 2010) 214–226, https://doi.org/10.1016/j.nano.2009.07.009.

[24] S. Aitekenov, et al., Raman, infrared and brillouin spectroscopies of biofluids for medical diagnostics and for detection of biomarkers, Crit. Rev. Anal. Chem. 0 (0) (Feb. 2022) 1–30, https://doi.org/10.1080/10408347.2022.2036941.

[25] D. Hu, et al., Detecting urine metabolites of bladder cancer by surface-enhanced Raman spectroscopy, Spectrochim. Acta A Mol. Biomol. Spectrosc. 247 (Feb. 2021), 119108, https://doi.org/10.1016/j.saa.2020.119108.

[26] H.M. Huttanus, et al., Raman chemometric urinalysis (Rametrix) as a screen for bladder cancer, PLoS One 15 (8) (Aug. 2020), e0237070, https://doi.org/10.1371/journal.pone.0237070.

[27] Y. Ma, J. Chi, Z. Zheng, A. Attygalle, I.Y. Kim, H. Du, Therapeutic prognosis of prostate cancer using surface-enhanced Raman scattering of patient urine and multivariate statistical analysis, J. Biophotonics 14 (1) (2021), e202000275, https://doi.org/10.1002/jbio.202000275.

[28] K. Gudun, Z. Elemessova, L. Khamkhash, E. Ralchenko, R. Bukasov, Commercial gold nanoparticles on untreated aluminum foil: versatile, sensitive, and cost-effective SERS substrate, J. Nanomater. 2017 (2017) 9182025, https://doi.org/10.1155/2017/9182025.

[29] Z. Kunushpayeva, A. Rapikov, A. Akhmetova, A. Sultangaziyev, D. Dossym, R. Bukasov, Sandwich SERS immunoassay of human immunoglobulin on silicon wafer compared to traditional SERS substrate, gold film, Sens. Bio-Sens. Res. 29 (Aug. 2020), 100355, https://doi.org/10.1016/j.sbsr.2020.100355.

[30] Z. Mukanova, K. Gudun, Z. Elemessova, L. Khamkhash, E. Ralchenko, R. Bukasov, Detection of paracetamol in water and urea in artificial urine with gold nanoparticle@Al foil cost-efficient SERS substrate, Anal. Sci. 34 (2) (2018) 183–187, https://doi.org/10.2116/analsci.34.183.

[31] A.R.M. Radzol, K.Y. Lee, W. Mansor, A. Azman, Optimization of Savitzky-Golay smoothing filter for salivary surface enhanced Raman spectra of non structural protein 1, in: TENCON 2014–2014 IEEE Region 10 Conference, Oct. 2014, pp. 1–6, https://doi.org/10.1109/TENCON.2014.7022409.

[32] S. Sergiienko, K. Moor, K. Gudun, Z. Yelemessova, R. Bukasov, Nanoparticle–nanoparticle vs. nanoparticle–substrate hot spot contributions to the SERS signal: studying Raman labelled monomers, dimers and trimers, Phys. Chem. Chem. Phys. 19 (6) (2017) 4478–4487, https://doi.org/10.1039/C6CP08254H.

[33] A. Arbuz, A. Sultangaziyev, A. Rapikov, Z. Kunushpayeva, R. Bukasov, How gap distance between gold nanoparticles in dimers and trimers on metallic and non-metallic SERS substrates can impact signal enhancement, Nanoscale Adv. 4 (1) (2022) 268–280, https://doi.org/10.1039/D1NA00114K.

[34] R.X. He, R. Liang, P. Peng, Y. Norman Zhou, Effect of the size of silver nanoparticles on SERS signal enhancement, J. Nanopart. Res. 19 (8) (Jul. 2017) 267, https://doi.org/10.1007/s11051-017-3953-0.

[35] K. Sugawa, et al., Particle size dependence of the surface-enhanced Raman scattering properties of densely arranged two-dimensional assemblies of Au(core)–Ag(shell) nanospheres, Phys. Chem. Chem. Phys. 17 (33) (Aug. 2015) 21182–21189, https://doi.org/10.1039/C4CP05058D.

[36] L.P. Moreira, L. Silveira, A.G. da Silva, A.B. Fernandes, M.T.T. Pacheco, D.D.F. M. Rocco, Raman spectroscopy applied to identify metabolites in urine of physically active subjects, J. Photochem. Photobiol. B Biol. 176 (Nov. 2017) 92–99, https://doi.org/10.1016/j.jphotobiol.2017.09.019.

[37] N.C. Dingari, G. Horowitz, J.W. Kang, R. Dasari, I. Barman, Raman spectroscopy provides a powerful diagnostic tool for accurate determination of albumin glycation, PLoS One 7 (Feb. 2012), e32406, https://doi.org/10.1371/journal.pone.0032406.

[38] M. Zong, et al., Comparison of surface-enhanced Raman scattering properties of serum and urine for the detection of chronic kidney disease in patients, Appl. Spectrosc. (Oct. 2020), https://doi.org/10.1177/0003702820966322, 0003702820966322.

[39] C. Chen, et al., Raman spectroscopy combined with multiple algorithms for analysis and rapid screening of chronic renal failure, Photodiagn. Photodyn. Ther. 30 (Jun. 2020), 101792, https://doi.org/10.1016/j.pdpdt.2020.101792.

[40] C.J. Saatkamp, M.L. de Almeida, J.A.M. Bispo, A.L.B. Pinheiro, A.B. Fernandes, L. S. Jr, Quantifying creatinine and urea in human urine through Raman spectroscopy aiming at diagnosis of kidney disease, JBO 21 (3) (Mar. 2016), 037001, https://doi.org/10.1117/1.JBO.21.3.037001.

[41] S. Kumar, S.K. Majumder, P.K. Gupta, H. Patidar, C.V. Kulkarni, Raman spectroscopy for estimation of urea in urine, in: 12th International Conference on Fiber Optics and Photonics (2014), paper T3A.65, Dec. 2014, https://doi.org/10.1364/PHOTONICS.2014.T3A.65. T3A.65.

[42] C. Hampton, D. Demoin, R.E. Glaser, Vibrational spectroscopy tutorial: sulfur and phosphorus, University of missouri, 2010. Fall.

[43] X. Hoccart, G. Turrell, Raman spectroscopic investigation of the dynamics of urea–water complexes, J. Chem. Phys. 99 (11) (Dec. 1993) 8498–8503, https://doi.org/10.1063/1.465626.

[44] R.L. Frost, J. Kristof, L. Rintoul, J.T. Kloprogge, Raman spectroscopy of urea and urea-intercalated kaolinites at 77 K, Spectrochim. Acta A Mol. Biomol. Spectrosc. 56 (9) (Aug. 2000) 1681–1691, https://doi.org/10.1016/S1386-1425(00)00223-7.

[45] R. Keuleers, H.O. Desseyn, B. Rousseau, C. Van Alsenoy, Vibrational analysis of urea, J. Phys. Chem. A 103 (24) (Jun. 1999) 4621–4630, https://doi.org/10.1021/jp984180z.

[46] J.A.M. Bispo, E.E. de Sousa Vieira, L. Silveira Jr., A.B. Fernandes, Correlating the amount of urea, creatinine, and glucose in urine from patients with diabetes mellitus and hypertension with the risk of developing renal lesions by means of Raman spectroscopy and principal component analysis, J. Biomed. Opt. 18 (8) (2013), 087004.

[47] T. Furukawa, et al., Raman microspectroscopy study of structure, dispersibility, and crystallinity of poly (hydroxybutyrate)/poly (l-lactic acid) blends, Polymer 47 (9) (2006) 3132–3140.

[48] E. Podstawka, M. Świątłowska, E. Borowiec, L.M. Proniewicz, Food additives characterization by infrared, Raman, and surface-enhanced Raman spectroscopies, Journal of Raman Spectroscopy: An International Journal for Original Work in all Aspects of Raman Spectroscopy, Including Higher Order Processes, and also Brillouin and Rayleigh Scattering 38 (3) (2007) 356–363.

[49] J. De Gelder, K. De Gussem, P. Vandenabeele, L. Moens, Reference database of Raman spectra of biological molecules, Journal of Raman Spectroscopy: An International Journal for Original Work in all Aspects of Raman Spectroscopy, Including Higher Order Processes, and also Brillouin and Rayleigh Scattering 38 (9) (2007) 1133–1147.

[50] J. De Gelder, et al., Monitoring poly (3-hydroxybutyrate) production in Cupriavidus necator DSM 428 (H16) with Raman spectroscopy, Anal. Chem. 80 (6) (2008) 2155–2160.

[51] G. Socrates, Infrared and Raman Characteristic Group Frequencies: Tables and Charts, John Wiley & Sons, 2004.

[52] J.B. Lambert, H.F. Shurvell, D.A. Lightner, R.G. Cooks, Introduction to Organic Spectroscopy, Macmillan Publishing Company, 1987.

[53] C.-H. Liu, et al., Raman, fluorescence, and time-resolved light scattering as optical diagnostic techniques to separate diseased and normal biomedical media, J. Photochem. Photobiol. B Biol. 16 (2) (1992) 187–209.
[54] M.M. Mossoba, Spectral Methods in Food Analysis, Marcel Dekker, 1999.
[55] C. Bayrak, S. Bayari, Vibrational and DFT studies of creatinine and its metal complexes, Hacettepe J. Biol. Chem 38 (2) (2010) 107–118.
[56] Z. Tao, L. Peng, P. Zhang, Y.-Q. Li, G. Wang, Probing the kinetic anabolism of poly-beta-hydroxybutyrate in cupriavidus necator h16 using single-cell Raman spectroscopy, Sensors 16 (8) (2016) 1257.
[57] C.M. Florkowski, Sensitivity, specificity, receiver-operating characteristic (ROC) curves and likelihood ratios: communicating the performance of diagnostic tests, Clin. Biochem. Rev. 29 (Suppl. 1) (Aug. 2008) S83–S87.
[58] K. Hajian-Tilaki, Receiver operating characteristic (ROC) curve analysis for medical diagnostic test evaluation, Caspian J Intern Med 4 (2) (2013) 627–635.
[59] J. Barratt, P. Topham, Urine proteomics: the present and future of measuring urinary protein components in disease, CMAJ 177 (4) (Aug. 2007) 361–368, https://doi.org/10.1503/cmaj.061590.
[60] E.J. Lamb, F. MacKenzie, P.E. Stevens, How should proteinuria be detected and measured? Ann. Clin. Biochem. 46 (3) (May 2009) 205–217, https://doi.org/10.1258/acb.2009.009007.
[61] C.B. Nielsen, H. Birn, F. Brandt, J.D. Kampmann, Urinary dipstick is not reliable as a screening tool for albuminuria in the emergency department—a prospective cohort study, Diagnostics 12 (Feb. 2022), https://doi.org/10.3390/diagnostics12020457 no. 2, Art. no. 2.
[62] D.E.E. Rizk, M.M. Agarwal, J.Y. Pathan, E.N. Obineche, Predicting proteinuria in hypertensive pregnancies with urinary protein-creatinine or calcium-creatinine ratio, J. Perinatol. 27 (5) (May 2007) 272–277, https://doi.org/10.1038/sj.jp.7211689.
[63] S. Kalantari, M. Nafar, S. Samavat, M. Parvin, B.F. Nobakht M.GH, F. Barzi, 1H NMR-based metabolomics exploring urinary biomarkers correlated with proteinuria in focal segmental glomerulosclerosis: a pilot study, Magn. Reson. Chem. 54 (10) (2016) 821–826, https://doi.org/10.1002/mrc.4460.
[64] C. Chen, et al., Urine Raman spectroscopy for rapid and inexpensive diagnosis of chronic renal failure (CRF) using multiple classification algorithms, Optik 203 (2020), https://doi.org/10.1016/j.ijleo.2019.164043.
[65] H. Yang, et al., Noninvasive and prospective diagnosis of coronary heart disease with urine using surface-enhanced Raman spectroscopy, Analyst 143 (10) (2018) 2235–2242, https://doi.org/10.1039/C7AN02022H.
[66] H.M. Huttanus, et al., Raman chemometric urinalysis (Rametrix) as a screen for bladder cancer, PLoS One 15 (8) (Aug. 2020) 1–21, https://doi.org/10.1371/journal.pone.0237070.